Chapter 13
Advances Toward Closed-Loop Deep Brain Stimulation

Stathis S. Leondopulos and Evangelia Micheli-Tzanakou

Abstract A common treatment for advanced stage Parkinsonism is the application of a periodic pulse stimulus to specific regions in the brain, also known as *deep brain stimulation* (or DBS). Almost immediately following this discovery, the idea of dynamically controlling the apparatus in a "closed-loop" or neuromodulatory capacity using neural activity patterns obtained in "real-time" became a fascination for many researchers in the field. However, the problems associated with the reliability of signal detection criteria, robustness across particular cases, as well as computational aspects, have delayed the practical realization of such a system. This review seeks to present many of the advances made toward closed-loop deep brain stimulation and hopefully provides some insight to further avenues of study toward this end.

13.1 Introduction

The uses of electrical stimulation and recording in medicine have a history dating back to the first century AD [95, 139, 121, 153, 76, 85, 21, 97, 138, 37, 30, 47]. However, since the first advances in microelectronics began to appear [7], medical electro-stimulation and recording equipment became portable and even implantable [23]. Soon after that, with the invention of the integrated circuit [84, 115], an ever-increasing number of components became available on a silicon chip of millimeter or even micron dimensions [107]. As a consequence, the availability and sophistication of electronic bio-implants began to greatly increase starting with the work of House [68] on the cochlear implant in 1969, the work of Humayun and de Juan [69] on the retinal implant in 1996, and the cortical implant reported by Donoghue [35] and Nicolelis [111] in 2002 and 2003.

S.S. Leondopulos
Rutgers University, Piscataway, USA, e-mail: stathis@ece.rutgers.edu

Evangelia Micheli-Tzanakou
Rutgers University, Piscataway, USA, e-mail: etzanako@rci.rutgers.edu

W. Chaovalitwongse et al. (eds.), *Computational Neuroscience*,
Springer Optimization and Its Applications 38, DOI 10.1007/978-0-387-88630-5_13,

Electrical stimulation of nuclei in the basal ganglia of the brain as a treatment for Parkinson's disease, also known as *deep brain stimulation* (or DBS), was approved by the US Food and Drug Administration and became commercially available in 1997 [151]. The apparatus consists of a stimulus generator implanted under the collar bone and a subcutaneous lead connecting the stimulator to an electrode fixed at the cranium and reaching the basal ganglia in the center of the human brain. Following implantation, a wireless link facilitates communication with the implant for the routine adjustment of the stimulus waveform by medical staff. In this manner, the treatment can be tuned or optimized over time while avoiding side effects. The neural signals emanating from the basal ganglia during DBS have been recorded and analyzed by Dostrovsky et al. [36], Wu et al. [162], Wingeier et al. [158], and Rossi et al. [130]. Moreover, there have been studies regarding the use of information contained in the neural activity of the basal ganglia as a control signal or regulator of the stimulus apparatus [106, 146, 134, 78, 39, 90, 12].

13.2 Nerve Stimulation

The simplest model of electrical nerve stimulation was introduced by Arvanitaki and uses the passive membrane model with membrane resistance R_m and capacitance C_m [4, 95]. In this scenario, assuming the stimulus current applied across the cell membrane is a constant I_s, then the change in transmembrane voltage becomes

$$V_\mathrm{m}(t) = I_\mathrm{s} R_\mathrm{m} \left(1 - e^{-t/R_\mathrm{m}C_\mathrm{m}}\right). \tag{13.1}$$

Moreover, given a threshold voltage ΔV_th, then the minimum stimulus current needed for the transmembrane voltage to reach ΔV_th is found for $t = \infty$ and is called the *rheobase current*:

$$I_\mathrm{rh} = \frac{\Delta V_\mathrm{th}}{R_\mathrm{m}}. \tag{13.2}$$

Also, another useful measure of stimuli is the time required to reach ΔV_th when $I_\mathrm{s} = 2I_\mathrm{rh}$. This is called *chronaxy* or *chronaxie* [95, 154] and is calculated as

$$t_\mathrm{c} = R_\mathrm{m} C_\mathrm{m} \ln 2. \tag{13.3}$$

As an example, Fig. 13.1 illustrates the decay of the minimum amplitude needed for stimulating a neuron as pulse width increases [99].

More sophisticated distributed models such as the core conductor model incorporate the shape of the neuron axon and conductivity of external media [24, 95]. Moreover, the shape and timing of stimuli are also influential as shown in detailed studies by Warman, McIntyre, Grill, and others [154, 99, 100, 54]. However, the passive membrane model with appropriate effective values for R_m and C_m remains a useful approximation for many applications [125, 74].

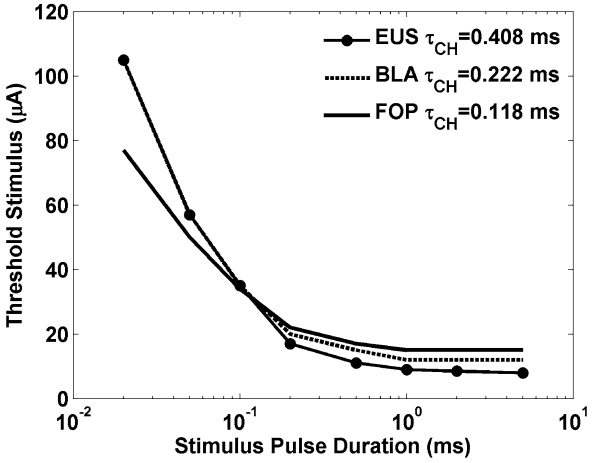

Fig. 13.1: Firing threshold of the external urethral sphincter motoneuron (EUS), the neuron innervating the bladder (BLA), and the fiber of passage in the white matter (FOP) stimulated with bipolar stimulation as predicted by simulation techniques and reported by McIntyre and Grill [99]. τ_{CH} represents the calculated chronaxie of the particular neuron).

13.3 Local Field Potentials

Measurable electrical phenomena that occur in the human body are due primarily to the transport of charged ions across the membrane of neurons as they relay and process information governing movement and perception. In particular, rapid changes in membrane permeability occurring on a millisecond scale produce current spikes or "action potentials" [9,65]. At the same time, thousands of synaptic junctions contribute to the "postsynaptic potential" or subthreshold changes in the transmembrane potential. Furthermore, random processes within the neuron membrane may cause spontaneous events to occur in addition to synaptic stimuli [81].

The *local field potential* (LFP) is related to the aggregate of the electric fields produced by individual neurons in the vicinity of the electrode within the dielectric medium of brain tissue. Furthermore, it is known that the recorded signal is influenced by a frequency filtering characteristic, so that only low-frequency elements of neural activity such as postsynaptic potentials propagate beyond the immediate cellular environment to produce measurable signals [11,10]. Also, characteristics of the analog front-end recording apparatus performing DC bias stability and prefiltering further modify the frequency band of the signal.

Bedard et al. [11, 10] have shown that the frequency-dependent attenuation with distance can be explained by using a nonhomogeneous model of extracellular dielectric properties that take into consideration the properties of neighboring neuron membranes. Also, at the macroscopic level, a comprehensive study of dielectric properties of tissues in the range of 10 Hz–20 GHz was prepared by

Gabriel et al. [45], including an empirical parametric model that fits well to the experimental data.

A more practical model for describing the dielectric properties at the neuroelectrode interface was developed by Johnson et al. [79]. In that study, an equivalent circuit model is used for explaining voltage-biasing effects of the recorded signal.

13.4 Parkinson's Disease

Parkinson's disease is due to the death or alteration of cells that produce the neurotransmitter dopamine in a region of the brain called *substantia nigra pars compacta* (SNc). In turn, the lack of dopamine weakens synaptic pathways between the SNc and the region called the striatum resulting in a general imbalance of activity within a group of brain nuclei collectively known as the basal ganglia [31]. As a result, the spike patterns of neurons in the *external globus pallidus* (GPe) become sparse, while the neurons in the *subthalamic nucleus* (STN) and *internal globus pallidus* (GPi) exhibit pronounced activity that is often in the form of synchronized oscillatory bursting [16, 92, 156, 71, 126]. Figures 13.2 and 13.3 show neural pathways of the basal ganglia as well as activity of key nuclei under normal physiological conditions and Parkinsonism, respectively. Moreover, dark arrows represent inhibitory synaptic pathways, gray arrows excitatory, and perforated arrows are pathways associated with dopamine. Externally, these processes are manifested as the Parkinsonian symptoms of essential tremor, muscle rigidity, bradykinesia (slowness of movement), and postural imbalance.

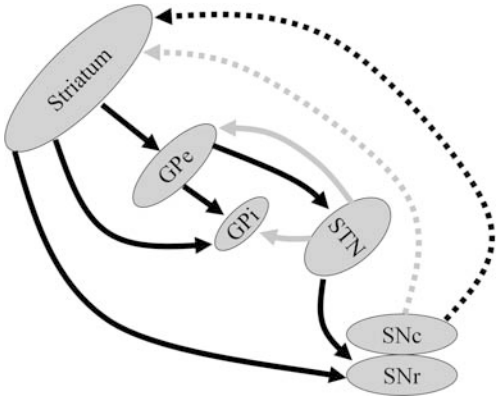

Fig. 13.2: Basal ganglia under normal conditions. This figure shows the nuclei in the basal ganglia and their synaptic paths including excitatory (*gray line*), inhibitory (*dark line*), and dopaminergic paths (*gray perforated line, dark perforated line*). A feedback loop between the STN and the GPe can be seen. This figure is modified from the figures reported by Gurney et al. [56] to emphasize changes due to dopamine depletion as described by Delong [31].

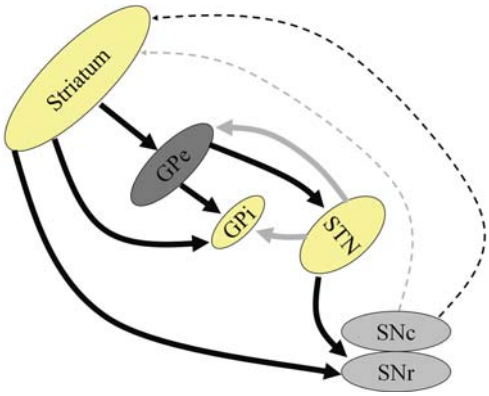

Fig. 13.3: Basal ganglia during a lack of dopamine (Parkinson's disease). Key nuclei and their synaptic paths including excitatory (*gray line*), inhibitory (*dark line*), and dopaminergic (*gray perforated line, dark perforated line*) paths are shown. *Dark-colored* nuclei signify diminished activity while *bright-colored* regions signify heightened activity. This figure is modified from the figures reported by Gurney et al. [56] to emphasize changes due to dopamine depletion as described by Delong [31].

13.4.1 Treatments

The treatment for early stage Parkinson's disease typically consists of the administration of levodopa (L-DOPA) orally. L-DOPA crosses the blood–brain barrier where it is converted into dopamine, thus restoring some of the movement capabilities to the patient. However, side effects that may emerge are dyskinesia (difficulty performing voluntary movements), depression, and psychotic episodes in some patients [28, 110].

Surgical procedures that have been used in the past as a treatment for advanced stage Parkinson's disease include pallidotomy, thalamotomy, and subthalamotomy [55]. In these procedures, functional MRI imaging techniques detect the location of specific nuclei in the brain of the patient. Following this, stereotactic surgical techniques are employed for the placement of electrodes at the target location. Next, electrode recordings are analyzed to achieve a more precise placement [59]. Finally, high temperatures $(80^{o}\mathrm{C})$ or electric currents are applied to cause destruction of cells (known as lesioning) in the STN or GPi.

The success of pallidotomies is hypothesized to be due to a reduction of activity in the GPi that is caused by the administrated (or artificially placed) lesions [84]. Furthermore, lesioning the STN with a subthalamotomy has a similar effect in the GPi because of the excitatory neuronal paths from the STN to the GPi [3]. Thus, lesions in the GPi simulate the inhibitory input to the STN and GPi that would otherwise be present under physiological conditions (see Figs. 13.2 and 13.3).

13.5 Deep Brain Stimulation

Electrical stimulation of the brain as a treatment for Parkinson's disease was first reported by Benabid et al. [13] in 1987. In particular, during stereotactic neurosurgery it was observed that stimulating the *ventral intermediate nucleus* (VIM) of the brain with a sequence of 1–2 V 0.5 ms pulses at 100 Hz blocked symptoms of the disease. Eventually, the lesioning procedures mentioned previously were replaced by the implantation of electrodes connected to a pulse generator. Moreover, the physician could tune the signal generator through a wireless link, thus adjusting the stimulus parameters.

13.5.1 DBS Mechanism

A primary contributing factor to the inhibitory effect of DBS on the STN and GPi is likely the release of adenosine by astrocytes as they are electrically stimulated [12]. Also, the same study reports how the inhibition is likely a combination of adenosine-related and "axonal" effects. That is, there are a number of hypotheses that attempt to explain the inhibitory effect of DBS on the STN and GPi. In particular, these are: (1) the blocking of action potentials by affecting properties of ion conductance in the neuron membrane, (2) the preferential stimulation of axons that terminate at inhibitory synapses rather than neurons themselves, and (3) the desynchronization of mechanisms occurring in the network as a whole. Out of these hypotheses, desynchronization seems to be the least refuted and least understood [101].

In practice, the effect of DBS on neural activity can be seen in recordings using extracellular electrodes that have been taken from patients during surgical implantation of DBS systems, as shown in Fig. 13.4. In particular, the work of Dostrovsky et al. [36] shows how the activity of pallidal neurons displays a period of quiescence after each stimulating pulse of DBS. Furthermore, the quiescent period increases with respect to the DBS pulse amplitude as can be seen in Fig. 13.5. Also, as the pulses become more dense at higher frequency stimulation, the quiescent periods seem to overlap, thus causing the inhibitory effect. A more macroscopic view of the effect of pulse amplitude is provided in Fig. 13.6 [162].

Figure 13.7 shows the neuron activity rate following a stimulus pulse measured as a percentage of the activity preceding the pulse (baseline activity). As can be seen in Fig. 13.7, neural activity is nearly 0 after the DBS pulse, but returns to normal firing after some time (between 50 and 100 ms).

13.5.2 Apparatus

All commercially available DBS systems are currently designed and manufactured by the Medtronic corporation. By name, the neurostimulators commonly used for

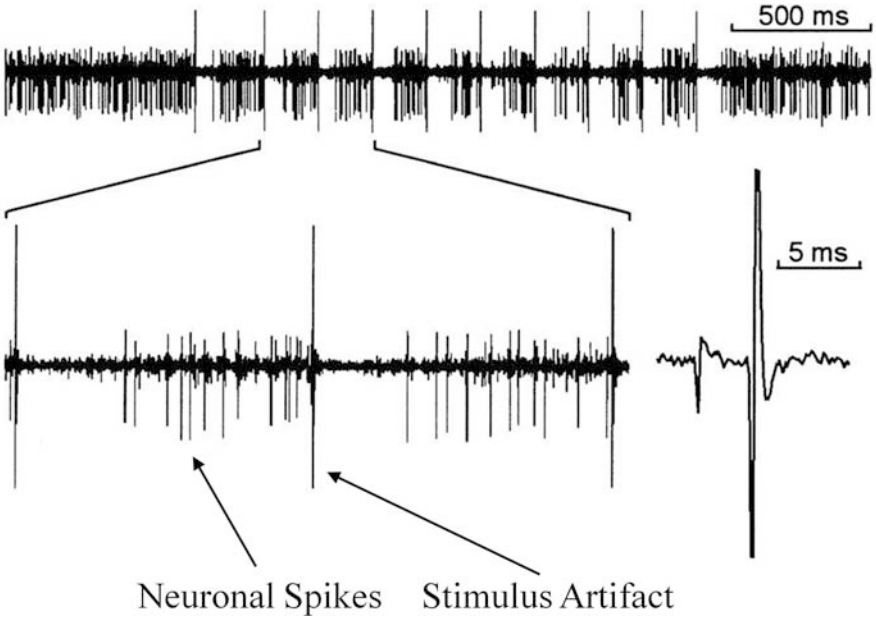

Fig. 13.4: Effects of DBS pulses on neural activity in the GPi as observed experimentally and reported by Dostrovsky et al. [36]. The larger *vertical line* segments are stimulus artifacts while the *shorter line* segments can be attributed to neuronal spike activity. A quiescent or inhibitory period during which there is no neuronal activity can be observed after each stimulus.

DBS are the "Itrel II Soletra," "Kinetra," and "Extrel" units (with Extrel used less frequently than the former two). Moreover, the specifications of the apparatus have been described in a number of publications [59, 101, 5, 89, 152]. Specifically, a 1.27 mm diameter probe with four 1.5 mm long contacts spaced 0.5 mm or 1.5 mm apart (depending on the version) is in contact with the target area of the brain and secured to the cranium at its base. Furthermore, a subcutaneous lead connects the base of the probe to a $53 \times 60 \times 10\,\mathrm{mm}^3$ neurostimulator implanted in the chest area under the collarbone of the patient [101].

The Extrel unit differs from the Soletra and Kinetra units in that an external stimulus generator communicates with the implant. In particular, the external apparatus generates the pulse waveform and then modulates it using a carrier frequency in the RF range. In turn, an implanted receiver demodulates the signal using passive circuit components including a capacitor [89, 137, 102].

13.5.3 Stimulus Specifications

The DBS units are capable of applying stimulus waveforms that consist of a train of pulses with the following specifications [152, 101]:

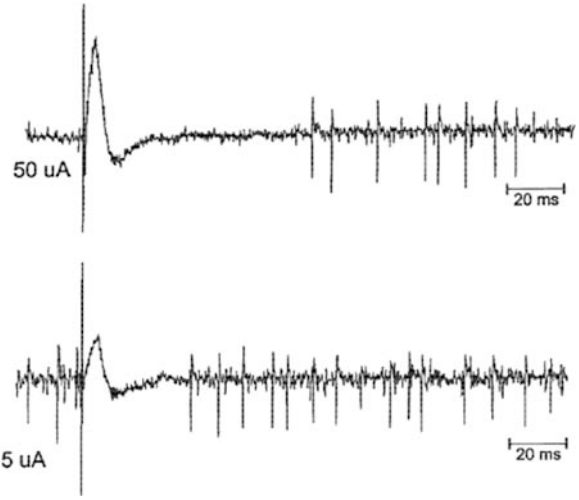

Fig. 13.5: Detail of the effects of a 50 and 5 μA DBS pulse of duration 150 μs on a single GPi neuron of a Parkinson's patient as observed experimentally and reported by Wu et al. [162]. The *tallest thin vertical line* segments are the stimulus artifacts, while the *shorter line* segments can be attributed to neuronal spike activity. A large pulse immediately followed by an inhibitory period is observed following the stimulus. Moreover, the smaller stimulus (5 μA) is followed by a short inhibitory period (roughly 30 ms), while the larger stimulus is followed by a longer inhibitory period (roughly 60 ms).

Pulse amplitude: 0–10.5 V (in steps of 0.1 V), and assuming a 1 kΩ load as reported, this means a 0–10.5 mA stimulation current.[1]

Pulse duration: 60–450 μs (1,000 μs maximum in the case of Extrel).

Pulse frequency: 2–185 Hz in the Soletra, 2–250 Hz in the Kinetra, and 2–1,000 Hz in the Extrel.

Pulse polarity: both monopolar and bipolar modes are available (only bipolar in the Extrel).

[1] The amplitude used in commercial DBS units (0–10.5 mA) is obviously much larger than what is reported in the experiments of Dostrovsky et al. [36], Hamilton et al. [60], and Lehman et al. [91], namely 5–100 μA. However, the current density turns out to be similar because of the differences in electrode diameter. In particular, the experimental work sited uses 25 μm (length) by 25–100 μm (diameter) electrodes, while commercial devices use a 1.5-mm (length) by 1.27-mm (diameter) electrodes.

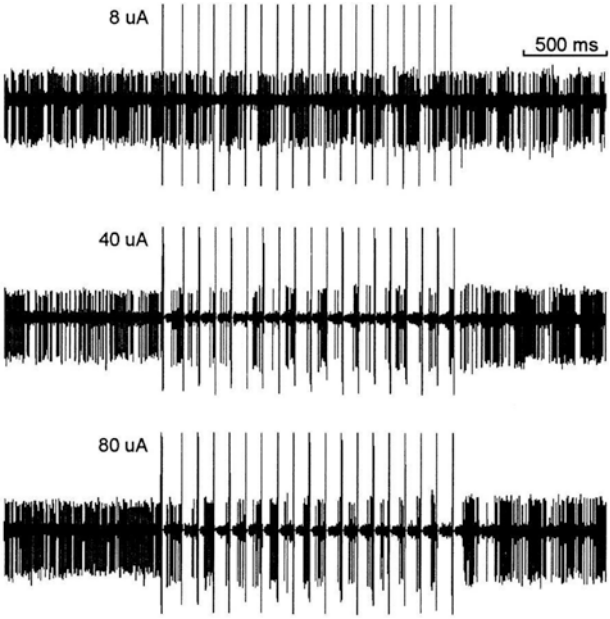

Fig. 13.6: Effects of DBS pulses (at 10 Hz) on a single GPi neuron in the GPi as observed experimentally and reported by Dostrovsky et al. [36]. The larger vertical line segments are stimulus artifacts, while the shorter line segments can be attributed to neuronal spike activity. It can be seen that as stimulus energy increases from 8 to 80 μA, the neural activity becomes more sparse.

13.5.4 DBS Programming

The typical procedure for programming DBS apparatus postoperatively begins with the determination of the "therapeutic window" of stimulation for each electrode [5, 152]. That is, using monopolar stimulus, keeping the pulse width at 60 μs and the frequency at 130 Hz, the pulse amplitude is increased from 0 V at increments of 0.2–0.5 V. Furthermore, the therapeutic window or range for a particular electrode is the set of amplitude values between the smallest therapeutic amplitude and the onset of undesirable side effects such as rigidity and dystonia (sustained muscle contractions). Next, the electrode with the largest therapeutic range is selected as the stimulus electrode [152].

Over the months following implantation, DBS parameters are modified according to the side effects and therapeutic results observed. Typically, the amplitude or frequency is increased as the patient develops a tolerance to the stimulus effect. Moreover, it is believed that a higher impedance or displacement of the electrodes due to glial tissue scarring is responsible for the diminishing effectiveness of DBS over the first postoperative months [40, 108]. In addition, long-term physiological processes

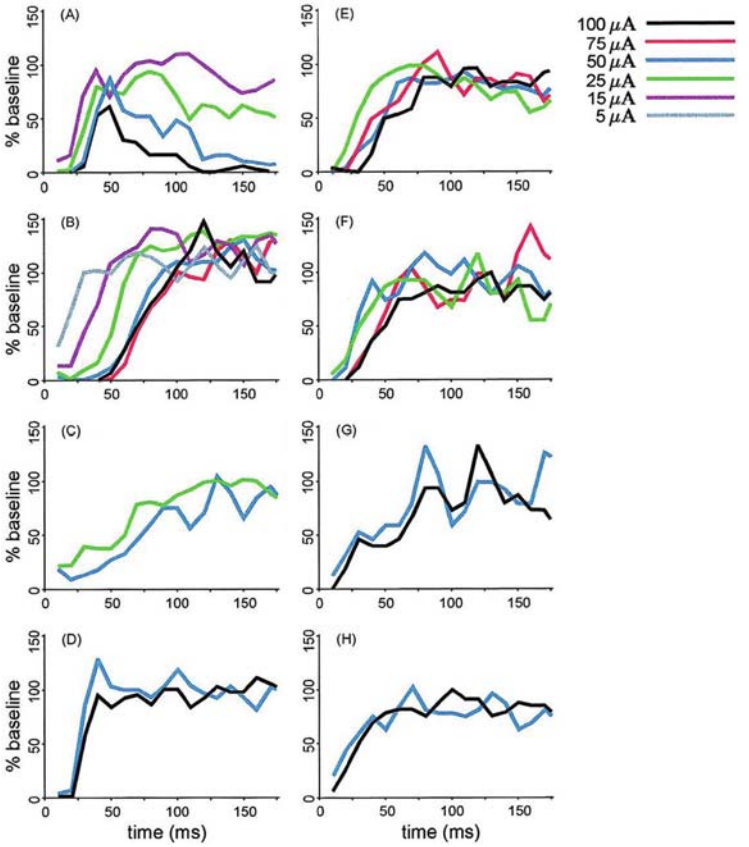

Fig. 13.7: Spike-rate in 10 ms bins, smoothed with a 20 ms sliding window, as percentage of baseline (no stimulus) and a function of time (stimulus at time 0) as observed experimentally and reported by Dostrovsky et al. [36]. A period of quiescence or inhibition can be seen immediately following a stimulus. Then, normal neural firing rates gradually resume.

influenced by neural activity cause the modification of synapses, thus strengthening or weakening the influence of one neuron on the behavior of another [140].

Increasing the pulse width is avoided due to the recruitment of and possible damage to adjacent brain centers and the resulting side effects such as dysarthria (a speech disorder) and ataxia (loss of movement coordination) [152, 99, 100]. For example, Fig. 13.8 shows curves of the minimum pulse width–amplitude combinations that cause tremor suppression and onset of adverse side effects as found through experimentation on human subjects. Moreover, this is a verification of the response of the theoretical lumped parameter model shown previously in Fig. 13.1.

In DBS, bipolar stimulation is avoided due to the higher power dissipation that it requires. Only if side effects persist, the bipolar mode turned on because of the

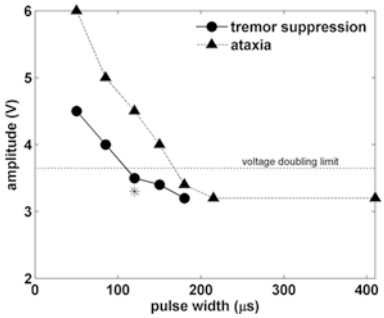

Fig. 13.8: Minimum pulse width–amplitude combinations causing tremor suppression and onset of adverse side effects as found experimentally and reported by Volkmann et al. [152]. The *asterisk* shows the pulse width suggested by Volkmann, while the voltage-doubling limit is a property of the Itrel II and Soletra stimulus generators reported by Volkmann.

more localized stimulation that it provides [5, 14]. At 6 months postoperatively, the stimulation parameters require only minor adjustments, as reported by Ashkan [5].

13.5.5 Side Effects

The undesirable side effects of DBS are primarily due to excess current leakage into adjacent brain centers and include cognitive degradation and severe emotional disturbances. However, other ill side effects may occur when DBS therapy is administered in conjunction with unrelated methods of diagnosis or treatment. For example, electrodes may be displaced by intense electromagnetic fields during MRI sessions, thus causing damage to brain tissue and displacing the location of the applied stimulus. Also, temperatures may become dangerously high during the administration of therapeutic diathermy (tissue heating), thus resulting in massive trauma or death [115, 131].

13.6 Biosignal Processing

All biological processes associated with perception and limb movement involve measurable electrical phenomena. Moreover, depending on where and how a measurement is taken, the recorded signal will exhibit particular characteristics [65, 144]. Typically, biosignal processing involves the analysis and classification of

recorded biosignals using any combination of signal processing techniques that are suitable for the particular application at hand [25]. In particular, the signal processing reduces the dimensionality of the data space by extracting useful information or "features" of the signal [29]. Thus, the high-dimensional recorded data is mapped to a lower dimensional "feature space." Moreover, the feature space is divided into regions or "classes" in order to categorize each measured signal.

13.6.1 Features

Biosignals can be analyzed using a large set of signal processing methods. However, some features are relatively simple to calculate while others are computationally demanding. Moreover, the issue of computational complexity becomes particularly important for integrated circuit implementations. Accordingly, Table 13.1 shows the computational complexities of various useful features in terms of signal sample size N, filter order n, decomposition levels L (for wavelets), number of signals m (PCA), lag q in terms of clock cycles, and the number of ALOPEX iterations c [29] (a blank "–" where present indicates that no studies were found).

Table 13.1: Feature extraction methods

Method	Complexity	Parallel and/or pipelined
Mean	$O(N)$	$O(\log(N))$
Variance	$O(2N)$	$O(2\log(N))$
FFT [124, 26]	$O(N\log(N))$	$O(\log(N))$
LPC (Levinson) [33, 87]	$O(nN+n^2)$	169 cycles/iteration
Wavelets (lifting) [93]	$O\left(4+2N\left(1-1/2^L\right)\right)$	–
Karhunen–Loeve with ALOPEX [29]	$O(2cN)$	$O(2c\log N)$
PCA – SGA [32]	Onm	$O(n^2)$
Third-order cumulant (skewness) [1]	$O(Nq^2+3qN)$	$O(N+q)$
Fourth-order cumulant (kurtosis) [96]	$O(N^6)$	–

[a] The 169 clock cycles (actually 3,378 per 20 iterations) for a pipelined multiplier implementation of the Levinson algorithm are reported in [136], however, there is no explicit mention of complexity in that paper. It seems evident, however, that for p multipliers in parallel, a pipelined implementation of the Levinson algorithm would be $O\left(\frac{N}{p}+n^2\right)$. Also, $O(L^4)$ is mentioned in [141] for fourth-order moments.

13.6.2 Classifiers

When some features of measured neural activity contain useful information that can be applied in regulating a stimulus generator, a method for automated classification may be in order. To this end, there are various methods that can be employed

broadly categorized as probability density estimation, nearest neighbor search, and neural networks [88, 66, 2]. In particular, probability density estimation or Bayes estimation categorizes the measurement in order to minimize the probability of error, nearest neighbor search finds the class that is associated with the nearest neighbors of the measurement, while neural networks consist of simple interconnected computational elements that have the end result of dividing the feature space into specific regions [59, 60, 58].

Among these classifiers, neural networks seem to be the most widely used methods in biomedical applications. However, choosing the best classifier as well as a feature set for a particular case is often an empirical task. Thus, a set or "ensemble" of different classifiers is often used for a single classification task [116].

13.6.3 Feature Selection

Selecting the features that minimize a cost function, such as the probability of misclassification, can be done exhaustively by examining each subset. However, this process is of complexity $\binom{N}{n}$ and may become intractable for large feature sets. Alternatively, there are a number of methods that reduce the complexity of the task, including "branch and bound," "sequential forward and backward selection," "Plus-l-take-away-r algorithm," and "max–min feature selection" [122, 19, 118].

13.7 Closed-Loop DBS

Following the discovery of the effects of electrical brain stimulation on the symptoms of Parkinson's disease [13] in 1987, investigations were initiated to explain how the stimulus achieved the desired result [101, 54]. Also, methods for administrating the newfound treatment as an implantable "brain pacemaker" were being explored [106, 146, 134, 54, 127, 78, 39]. In particular, the first disclosure of such an apparatus was the original patent on DBS filed by Rise and King [127] of the Medtronic corporation in 1996, where a system consisting of an electrode sensor, a microprocessor, stimulus generator, and additional peripheral circuitry was proposed for the purpose of measuring tremor-related symptoms in the arm and adjusting stimulus parameters based on the measurements. Subsequently, another patent was filed by John [78] in 2000, elaborating on the original proposal by including provisions for multiple sensors such as electrodes implanted in the brain and/or surface electrodes on the scalp and limbs. In addition, John proposed particular signal processing methods for assessing the measured data including the computation of signal variance, correlation, discrete Fourier transform, peak detection, and Mahalanobis distance or Z-scores. Also, provisions for wireless data telemetry to an external PC or handheld processor were included in that patent.

In the scientific literature, improvements to DBS have been suggested by a number of authors [106, 146, 134, 39]. In particular, Montgomery and Baker [106] suggested that a future direction of DBS would be to incorporate the ability of acquiring and decoding neurophysiological information "to compute the desired action." Also, using results from a mathematical model of interconnected phase oscillators, Tass [146] proposes a method of demand-controlled double-pulse stimulation that would hypothetically enhance the effectiveness of DBS while reducing the power consumption of a stimulator in the long term. In addition, Sanghavi [134] and Feng et al. [39] propose methods for adaptively modifying stimulus parameters while seeking to minimize measures of brain activity in the vicinity of the implant.

13.7.1 Demand-Controlled DBS

From a theoretical perspective, Tass established a stimulus methodology based on a model of Parkinsonian brain activity [146, 147]. In particular, Tass simulated the synchronized oscillatory behavior of the basal ganglia using a network of phase oscillators. This method is as follows: given N oscillators with global coupling strength $K > 0$ where the phase, stimulus intensity, and noise associated with the jth oscillator are Ψ_j, I_j, and $F_j(t)$, respectively, the behavior of the jth oscillator and its relation to other oscillators as well as the stimulus is shown in Equations (13.4), (13.5), and (13.6). In particular, defining factors $S_j(\Psi_j)$ and $X_j(t)$ as

$$S_j(\Psi_j) = I_j \cos(\Psi_j) \text{ and} \tag{13.4}$$

$$X_j(t) = \begin{pmatrix} 1\text{: neuron}_j \text{ is stimulated} \\ 0\text{: otherwise} \end{pmatrix}, \tag{13.5}$$

the rate of change of the jth phase oscillator is given by

$$\dot{\psi} = \Omega - \frac{K}{N} \sum_{k=1}^{N} \sin(\psi_j - \psi_k) + X_j(t) S_j(\psi_j) + F_j(t). \tag{13.6}$$

Tass showed that the model in Equations (13.4), (13.5), and (13.6) is able to generate patterns of both synchronized oscillatory firing and random nonoscillatory behavior. Moreover, the network tends to remain in a synchronized oscillation until a global stimulus is applied at time t_0 so that $X_j(t_0) = 1$ for all j.

Effective stimulation methods for suppression of abnormal burst activity in this model, as reported by Tass, include low-amplitude high-frequency stimulation (20 times the burst frequency), low-frequency stimulation (equal to the burst frequency), or a single high-amplitude pulse, with the high-amplitude pulse being the most effective when it is applied at the appropriate phase of each neuron. Furthermore, Tass proposes a demand-controlled stimulation technique whereby the synchronicity

among individual oscillators is measured, and when passing a predefined threshold, it activates a stimulation pulse.

In order to detect synchronicity among neurons, Tass proposes the calculation of cluster variables – the center of gravity in phase space of all oscillators. Specifically, if $R_m(t)$ and $\phi_m(t)$ are the magnitude and phase respectively of the center of gravity of m clusters, and Ψ_j is the phase of the jth oscillator, then the cluster variable is

$$Z_m(t) = R_m(t)e^{i\phi_m(t)} = \frac{1}{N}\sum_{j=1}^{N} e^{im\psi_j(t)}. \tag{13.7}$$

Thus, if the magnitude of the cluster variable is close to 0, there is very little synchronicity, but when it is close to unity, there is high synchronicity.

13.7.2 ALOPEX and DBS

Sanghavi [134] proposed an integrated circuit (IC) design of an adaptive DBS system where power estimation of recorded neural activity is used as a global "error measure" that drives the modification of stimulus pulse width, amplitude, and frequency of multiple signal generators. Furthermore, the modification is accomplished in simulation with minimal power requirements (roughly 0.8 mW) using an analog design of the stochastic optimization algorithm ALOPEX.

Since its application to BCI [150, 62, 105, 38], the ALOPEX algorithm was applied to numerous studies involving image pattern recognition and artificial neural networks [29]. The algorithm itself is based on the principle of Hebbian learning wherein the synaptic strength between two neurons increases in proportion to the correlation between the activities of those neurons [140]. Similarly, given a set of modifiable variables at iteration k, $b_k = \{b_{1,k}, b_{2,k}, , b_{N,k}\}$, and a global response estimate R_k, ALOPEX recursively modifies each $b_{j,k}$ by using correlation measures between previous changes in $b_{j,k}$ and changes in R_k. Moreover, to keep the algorithm from falling into an infinite loop, stochastic noise $r_{j,k}$ is included. Finally, given stochastic and deterministic step sizes $\sigma_{j,k}$ and $\sigma_{j,k}$, a reformulation of the algorithm in its most simplified "parity" form, as it is described in [62], is

$$d_{j,k} = \frac{(R_{k-1} - R_{k-2})}{|R_{k-1} - R_{k-2}|} \cdot \frac{(b_{j,k-1} - b_{j,k-2})}{|b_{j,k-1} - b_{j,k-2}|}, \tag{13.8}$$

$$b_{j,k} = b_{j,k-1} + \gamma_{j,k} \cdot d_{j,k} + \sigma_{j,k} \cdot r_{j,k}. \tag{13.9}$$

Subsequently, new versions were developed including the 2T-ALOPEX algorithm contributed by Sastry et al. [135] and the ALOPEX-B algorithm contributed by Bia [18]. In particular, 2T-ALOPEX incorporates explicit probability distributions into the calculation of each iteration, while ALOPEX-B is a similar but

simplified version of 2T-ALOPEX. Finally, Haykin et al. [63] improved convergence by combining the original formulation with that of Bia. Moreover, Haykin et al. provide a good contextual introduction and derivation of ALOPEX, while Sastry et al. prove that 2T-ALOPEX behaves asymptotically as a gradient-descent method. Also, Meissimilly et al. [103] introduced parallel and pipelined implementations of ALOPEX applied to template matching with corresponding computational and temporal complexities of calculating the global response function R_k.

13.7.3 Genetic Algorithms and DBS

Feng et al. [39] use a model by Terman et al. [149] to test a method of stimulus administration where each stimulus parameter is obtained from a distribution of such measures, thus incorporating a degree of randomness in the stimulus waveform. Moreover, in this method, the shape of each distribution curve is a piecewise linear model where the model parameters are modified by a genetic algorithm that seeks to reduce the cross-correlation and/or autocorrelation of measurements taken from multiple sensors. Figure 13.9 shows a diagram of the method proposed by Feng et al.

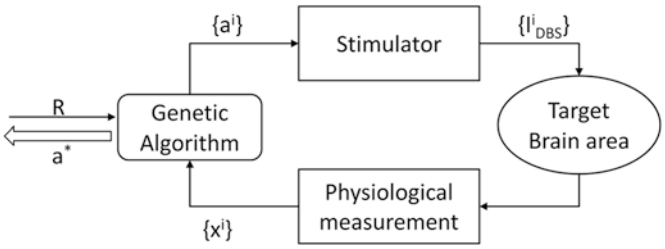

Fig. 13.9: The method proposed by Feng et al. [39] to draw deep brain stimulation parameters (I^i_{DBS}) from distributions whose shape descriptors (a^i) are selected by a genetic algorithm that seeks to minimize correlations in measured data (x^i). Constraints (R) on the genetic algorithm may be imposed externally.

13.7.4 Hardware Implementations

Various components of a closed-loop system have been implemented as a microelectronic design, including power and telemetry components [159], and stimulus/recording circuits interfacing with an external computing platform [90]. A typical setup for the real-time transmission of biosignals from a neural implant is shown in Fig. 13.10 [159].

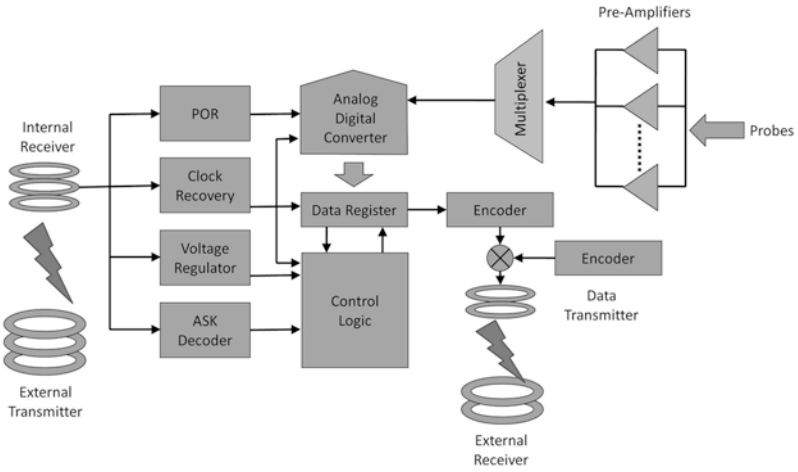

Fig. 13.10: A system for recording and decoding neuron activity. Power and data are transmitted through wireless telemetry [159].

13.8 Related Advances in Other Neuroprosthetic Research

Real-time biosignal processing has also advanced in other applications of neural prostheses in addition to DBS, such as cardiac pacemakers [133], retinal and cochlear implants [123, 69, 144], and brain-to-computer interfaces (BCI) [150, 62, 48, 91, 132, 161, 155, 49, 46]. In particular, pattern recognition systems for detecting abnormal heart activity have been proposed for cardiac pacemaker technology [133, 86]. Also, the decoding of neural activity in the premotor cortex of the brain to control robotic limbs has been successfully implemented in experiments with primates [111, 35]. Moreover, wireless telemetry and power transfer to implanted circuitry have been successful for cochlear and retinal implants [109]. There has also been research on detecting epileptic seizures and building an artificial hypocampus [72, 15].

Retinal and cochlear implants are relevant to DBS because of their wireless power transfer and data telemetry capabilities [123, 69, 144], while real-time signal processing of biosignals seems to have advanced more in cardiac pacemaking [6, 103, 128, 42] and especially BCI systems [150, 62, 48, 91, 132, 161, 155, 49, 46].

A typical setup for the real-time transmission of biosignals from a neural implant includes sensors (chemical or electrode) for detecting neural activity, signal processing for coding the activity, and communications circuitry for transmitting the information as shown in Fig. 13.10. In addition, the need for analog amplifiers, filters, and stimulus generators is ubiquitous among these designs [159]. Thus, methods included in the preprocessing and stimulus pulse generation stages have

also been proposed including amplifier designs [50, 117, 52], analog-to-digital conversion (A/D) [51], and voltage multiplier designs [113].

13.8.1 Closed-Loop Cardiac Pacemaker Technology

Some research in cardiac pacemaker technology has sought to modify stimulus parameters in response to measured neural activity. Moreover, this notion of autonomous regulation is similar in principal to adaptive, autonomous, or closed-loop *deep brain stimulation* (DBS).

The current standard for signal processing in cardiac pacemaking still consists of a simple band-pass filter with adaptive threshold detection [6, 103, 128]. However, new methods have been proposed that also include nonlinear filtering, wavelet analysis, and linear regression as well as threshold detection [86,128,42]. For example, Rodrigues et al. [128] implement filter banks (wavelets) with linear regression and threshold techniques in an IC design for detecting "R-waves" in cardiograms. In particular, given an input waveform $x(n)$ and wavelet filter H, the output of the wavelet decomposition is

$$y(n) = x(n)^T H. \tag{13.10}$$

Next, the "decision signal" is computed as

$$T(n) = x(n)^T H (H^T H)^{-1} H^T x(n). \tag{13.11}$$

Finally, the detection of the R-wave is considered positive if for some $\beta > 0$ and maximum decision signal $T_{\max}$, $T(n) \geq \beta T_{\max}$. Furthermore, complexity of the algorithm is $O(N)$, while the circuit design reported in [128] requires 6 multiplications and 45 summations per iteration and achieves a performance of roughly 99% correct detection and less than 1% false alarm.

13.8.2 Brain-to-Computer Interface

The first reported brain-to-computer interface (BCI) employing an adaptive algorithm and feedback was reported by Tzanakou et al. [150, 105, 38] where pixels on a screen were modified by the ALOPEX algorithm [62] to excite particular neurons (or receptive fields) in the visual pathway of a frog brain. Recently, BCI methods have been reported for detecting intended movements of primates. These include linear methods such as the "population vector" algorithm [48], finite impulse response (FIR) filters [132], Kalman filtering [161], nonlinear methods such as neural networks (NN) including time-delay NN's (TDNN) [155], gamma models [49] and recurrent NN's [132], and probabilistic approaches such as Bayesian inference [46]. Moreover, the nonlinear methods tend to achieve more accurate results at the expense of computational complexity.

In the case of linear methods, a typical formulation consists of sampling neuron spike-counts at intervals of 50 ms from multiple (15) recording sites. Moreover, the training stage consists of sampling roughly 1 s of data (20 intervals) and storing this information into a matrix $R_{(20\times15)}$ while storing the resulting hand position in terms of $x-y$ coordinates into a vector k. Next, the filter is constructed as $f=(R^TR)^{-1}R^Tk$ and the reconstruction of movement for a history of neural activity R is obtained as $u=R\times f$.[2] In addition, there are more sophisticated formulations that take into account the velocity and acceleration of the movement as well as prior information about the behavior of neurons in the cortex [82].

Almost all reported BCI methods utilize the same preprocessing stage that consists of spike detection, sorting, and counting over an interval typically in the range of 50–100 ms. Moreover, correlation methods and principal component analysis (PCA) with threshold detection are reported as methodologies for the spike detection [22, 80]. However, Wessberg et al. [155] report using straight linear regression with no spike detection.

13.9 Neural Network Modeling and the Basal Ganglia

The neurocomputational aspects of Parkinson's disease and DBS have been examined using neural network models. Aside from their usefulness as classifiers [129, 98, 67], static neural networks have been used to model the basal ganglia and the outcome of pallidotomies [60, 58, 104]. In addition, the temporal characteristics of neurons in these areas and the effects of DBS on neural activity have been investigated using dynamic, pulsed, or spiking neural networks [56, 57, 53, 17, 43, 44, 70, 149, 54, 8]. The models employed typically include Hodgkin–Huxley formulations as well as larger networks of simpler integrate-and-fire units [70]. However, there is a plethora of models that range in complexity and accuracy that may be used to this end, such as the Noble [112] and Fitzhugh-Nagumo [41] models, as well as many others [136, 61, 64, 160, 157, 143, 141, 27, 73, 75].

Three general methods of modeling nuclei of the basal ganglia can be found in the scientific literature. These can be broadly categorized into "functional" models that are designed to provide insight into the computational function of the basal ganglia [56, 57, 53, 17, 43, 44, 142, 8], "physiological" models that incorporate more details of ion transport [70, 149, 54], and "conceptual" models [20, 77, 145, 34, 148] that provide a description of the synaptic connectivity. Moreover, the physiological models have been used in simulations of applied deep brain simulation (DBS). In particular, Grill et al. [54] show that extrinsic high frequency stimulation "masks" or

[2] The formulation is included here as it appears in the literature. However, there are some unresolved questions. In particular, it would seem that a separate filter would be required for each movement element so that given a history of 20 positions, there are corresponding x and y-coordinate vectors x and y of 20 elements each. In that case, two filters would be derived as $f_x=(R^TR)^{-1}R^Tx$ and $f_y=(R^TR)^{-1}R^Ty$. Then, given a set of new data S in the testing phase, the corresponding hand positions would be given as $x_{\text{new}}=S\times f_x$ and $y_{\text{new}}=S\times f_y$.

prevents internal activity of single neurons from being expressed at the output, thus causing an "informational lesion," while Feng et al. [39] use a model by Terman et al. [149] to test a novel method of stimulus administration. Also, in response to in vitro studies of the rat GPe and STN [120], Humphries and Gurney [70] design models that reproduce the oscillatory and bursting modality of the neural circuits. In addition, an analog CMOS model of Parkinsonian activity has been investigated by Sridhar [142].

13.10 Summary

Overall, various methods for implementing a closed-loop neuromodulator have been presented including conceptual schemes in simulation as well as hardware designs facilitating the goal. Also, both experimental and simulation studies have provided some insight into the neural mechanisms involved in the success of DBS. However, there remains a need for some performance criteria in deciding which method of closed-loop DBS will be the most successful. To this end, some preliminary comparisons of computational complexity are merely a starting point. What is needed is a rigorous test on animal and human subjects including quantitative measures of success in reducing symptoms while avoiding side effects. Ultimately, the progress will depend on what is (or is not) approved by organizations such as the United States (US) Food and Drug Administration (FDA) [119].

References

1. Ahmed, R.E., Al-Turaig, M.A., Alshebeili, S.A. VLSI architecture for computing third-order cumulants, Int J Electron **77**(1), 95–104 (1994)
2. Alippi, C., Braione, P. Classification methods and inductive learning rules: What we may learn from theory. IEEE Trans Syst, Man, Cybern C Appl Rev **31**(4), 364–378 (2006)
3. Alvarez, L., Macias, R., Guridi, J., Lopez, G., Alvarez, E., Maragoto, C., Teijeiro, J., Torres, A., Pavon, N., Rodriguez-Oroz, M.C., Ochoa, L., Hetherington, H., Juncos, J., De Long, M.R., Obeso, J.A. Dorsal subthalamotomy for Parkinsons disease. Mov Disord **16**(1), 72–78 (2001)
4. Arvanitaki, A. Les variations gradues de la polarisation des systmes excitables, Thesis, University Lyons, Hermann et cie, Paris, 1938.
5. Ashkan, K., Wallace, B., Bell, B.A., Benabid, A.L. Deep brain stimulation of the subthalamic nucleus in Parkinsons disease 1993 2003: Where are we 10 years on? Br J Neurosurg **8**(1), 19–34 (Feb 2004)
6. Bai, J., Lin, J. A pacemaker working status telemonitoring algorithm. IEEE Trans Inform Technol Biomed **3**(3) (Sep 1999)
7. Bardeen, J., Brattain, W.H. The transistor, a semiconductor triode. Phys Rev **74**(2), 230 (1948)
8. Barto, A.G. Adaptive critic and the basal ganglia. In Houk, J.C., Davis, J.L., Beiser, D.G. (eds.) Models of Information Processing in the Basal Ganglia, pp. 215–232. MIT Press, Cambridge (1995)

9. Bear, M.F., Connors, B.W., Pardiso, M.A. Neuroscience: Exploring the Brain. LippincottWilliams & Wilkins, Philadelphia (2001)
10. Bedard, C., Kroger, H., Destexhe, A. Model of low-pass filtering of local field potentials in brain tissue. Phys Rev E – Stat Nonlin Soft Matter Phys **73**(5), 051911 (2006)
11. Bedard, C., Kroger, H., Destexhe, A. Modeling extracellular field potentials and the frequency-filtering properties of extracellular space. Biophys J **86**, 1829–1842 (March 2004)
12. Bekar, L., Libionka, W., Tian, G., et al. Adenosine is crucial for deep brain stimulation mediated attenuation of tremor. Nat Med 14(1), 7580.s (2008)
13. Benabid, A.L., Pollak, P., Louveau, A., Henry, S., de Rougemont, J. Combined (thalamotomy and stimulation) stereotactic surgery of the VIM thalamic nucleus for bilateral Parkinson disease. Appl Neurophys **50**(16), 34–46 (1987)
14. Benabid, A.L. Deep brain stimulation for Parkinson's disease, Curr Opin Neurobiol, **13**, 696–706 (2003)
15. Berger, T.W. Implantable biomimetic microelectronics for the replacement of hippocampal memory function lost due to damage or disease. IEEE International Joint Conference on Neural Networks, Vol. 3, pt.3. p. 1659 (2004)
16. Bergman, H., Wichmann, T., Karmon, B., DeLong, M.R. The primate subthalamic nucleus. II. Neuronal activity in the MPTP model of Parkinsonism. J Neurophysiol **72**(2), 507–520 (Aug 1994)
17. Berns, G.S., Sejnowski, T.J. A computational model of how the basal ganglia produce sequences. J Cogn Neurosci **10**(1), 108–121 (1998)
18. Bia, A. ALOPEX-B: A new, simple but yet faster version of the ALOPEX training algorithm, Int J Neural Syst **11**(6), 497–507 (2001)
19. Bluma, A.L., Langley, P. Selection of relevant features and examples in machine learning. Artif Intell **97**, 245–271 (1997)
20. Brown, J.W., Bullock, D., Grossberg, S. How laminar frontal cortex and basal ganglia circuits interact to control planned and reactive saccades. Neural Netw, **17**, 471–510 (2004)
21. Cavallo, T. An Essay on the Theory and Practice of Medical Electricity. Printed for the author, London (1780)
22. Chapin, J.K., Moxon, K.A., Markowitz, R.S., Nicolelis, M.A.L. Real-time control of a robot arm using simultaneously recorded neurons in the motor cortex. Nat Neurosci, **2**(7) (July 1999)
23. Chardack, W., Gage, A., Greatbatch, W. A transistorized, self-contained, implantable pacemaker for the long-term correction of complete heart block. Surgen **48**, 543 (1960)
24. Clark, J., Plonsey, R. A mathematical evaluation of the core conductor model. Biophys J **6**, 95 (1966)
25. Coatrieux, J.L. Integrative science: Biosignal processing and modeling. IEEE Eng Med Biol Mag **23**(3), 9–12 (May–June 2004)
26. Cooley, J.W., Tukey, J.W. An algorithm for the machine calculation of complex Fourier series, Math Comput **19**, 297–301 (1965)
27. Coop, A.D., Reeke, G.N., Jr. The composite neuron: A realistic one-compartment Purkinje cell model suitable for large-scale neuronal network simulations. J Comput Neurosci **10**(2), 173–186 (2001)
28. Cotzias, G.C., VanWoert, M.H., Schiffer, L.M. Aromatic amino acids and modification of parkinsonism. N Engl J Med **276**, 374–379 (1967)
29. Dasey, T.J., Micheli-Tzanakou, E. Fuzzy neural networks. In: Micheli-Tzanakou, E. (ed.) Supervised and Unsupervised Pattern Recognition Feature Extraction and Computational Intelligence, pp. 135–162. CRC Press, LLC (2000)
30. De Forest, L. Device for amplifying feeble electrical currents, US Patent #841387 (1907)
31. DeLong, M.R. Primate models of movement disorders of basal ganglia origin, Trends Neurosci **13**, 281–285 (1990)
32. Dehaene, J., Moonen, M., Vandewalle, J. An improved stochastic gradient algorithm for principal component analysis and subspace tracking. IEEE Trans Signal Process **45**(10) (Oct 1997)

33. Delsarte, P., Genin, Y. On the splitting of the classical algorithms in linear prediction theory. IEEE Trans Acoust **ASSP-35**(5) (May 1987)
34. Djurfeldt, M., Ekeberg, O., Graybiel, A.M. Cortex-basal ganglia interaction and attractor states. Neurocomputing **3840**, 573–579 (2001)
35. Donoghue, J.P. Connecting cortex to machines: Recent advances in brain interfaces, Nat Neurosci Suppl **5** (Nov 2002)
36. Dostrovsky, J.O., Levy, R., Wu, J.P., Hutchison, W.D., Tasker, R.R., Lozano, A.M. Microstimulation-induced inhibition of neuronal firing in human globus pallidus. J Neurophys **84**, 570–574 (Jul 2000)
37. Du Bois-Reymond, E. Untersuchungen ber thierische elektricitt. G. Reimer, Berlin (1848)
38. Tzanakou, E. Principles and Design of the ALOPEX Device: A Novelmethod of Mapping Visual Receptive Fields, Ph.D. dissertation, Syracuse University, Department of Physics (1977)
39. Feng, X., Greenwald, B., Rabitz, H., Shea-Brown, E., Kosut, R. Toward closed-loop optimization of deep brain stimulation for Parkinson's disease: Concepts and lessons from a computational model. J Neural Eng **4**, L14–L21 (2007)
40. Fitch, M.T., Doller, C., Combs, C.K., Landreth, G.E., Silver, J. Cellular and molecular mechanisms of glial scarring and progressive cavitation: In vivo and in vitro analysis of inflammation-induced secondary injury after CNS trauma. J Neurosci **19**(19), 8182–8198, Oct 1 (1999)
41. Fitz Hugh, R. Impulses and physiological states in theoretical models of nerve membrane. Biophys J **1**(6), 445–466 (1961)
42. Friesen, G., Jannett, T., JadallahM., Yates, S., Quint, S., Nagle, H. A comparison of the noise sensitivity of nine QRS detection algorithms. IEEE Trans Biomed Eng **37**(1), 85–98 (Jan 1990)
43. Fukai, T. Modeling the interplay of short-term memory and the basal ganglia in sequence processing. Neurocomputing **26–27**, 687–692 (1999)
44. Fukai, T. Sequence generation in arbitrary temporal patterns from theta-nested gamma oscillations: A model of the basal ganglia-thalamo-cortical loops. Neural Netw **12**(7–8), 975–987 (1999)
45. Gabriel, S., Lau, R.W., Gabriel, C. The dielectric properties of biological tissues: III. Parametric models for the dielectric spectrum of tissues. Phys Med Biol **41**, 2271–2293 (1996)
46. Gao, Y., Blacky, M.J., Bienenstock, E., Shoham, S., Donoghue, J.P. Probabilistic inference of hand motion from neural activity in motor cortex. Adv Neural Inf Process Syst **14**, 213–220 (2002)
47. Gasser, H.S., Erlanger, J. A study of the action currents of the nerve with the cathode ray oscillograph. Am J Physiol **62**, 496–524 (1922)
48. Georgopoulos, A., Schwartz, A., Kettner, R. Neural population coding of movement direction. Science **233**, 1416–1419 (1986)
49. Georgopoulos, A.P., Lurito, J.T., Petrides, M., Schwartz, A.B., Massey, J.T. Mental rotation of the neuronal population vector. Science, **243**, 234–236 (1989)
50. Gerosa, A., Maniero, A., Neviani, A. A fully integrated dual-channel logdomain programmable preamplifier and filter for an implantable cardiac pacemaker, IEEE Transactions on Circuits and Systems. I: Regular Papers, **51**(10) (Oct 2004)
51. Gerosa, A., Maniero, A., Neviani, A. A fully integrated two-channel a/d interface for the acquisition of cardiac signals in implantable pacemakers. IEEE J Solid-State Circuits **39**(7), July (2004)
52. Ghovanloo, M., Najafi, K. A Modular 32-site wireless neural stimulation microsystem. IEEE J Solid-State Circuits **39**(12), 2457–2466 (2004)
53. Gillies, A., Arbuthnott, G. Computational models of the basal ganglia, Mov Dis **15**(5), 762–770 (2000)
54. Grill, W.M., Snyder, A.N., Miocinovic, S. Deep brain stimulation creates an informational lesion of the stimulated nucleus. Neuroreport **15**(7), 1137–1140, May 19 (2004)
55. Guridi, J., Lozano, A.M. A brief history of pallidotomy. Neurosurgery **41**(5), 1169–1180 (1997)

56. Gurney, K., Prescott, T.J., Redgrave, P. A computational model of action selection in the basal ganglia. I. A new functional anatomy. Biol Cybern **84**(6), 401–410 (2001)
57. Gurney, K., Prescott, T.J., Redgrave, P. A computational model of action selection in the basal ganglia. II. Analysis and simulation of behaviour. Biol Cybern **84**(6), 411–423 (2001)
58. Hamilton, J. Analysis of physiological function in the globus pallidus with neural networks, (PhD-MD) Jan (2000)
59. Hamilton, J.L., Micheli-Tzanakou, E., Lehman, R. Analysis of electrophysiological data in surgical treatment for Parkinson's disease. Proceedings of the 24th IEEE Northeast Conference on Bioengineering, pp. 5–6 (1998)
60. Hamilton, J.L., Micheli-Tzanakou, E., Lehman, R.M. Neural networks trained with simulation data for outcome prediction in pallidotomy for Parkinson's disease. IEEE Eng Med Biol Soc Conf **1**, 1–4 (2000)
61. Hanson, F.B., Tuckwell, H.C. Diffusion approximation for neuronal activity including reversal potentials. J Theor Neurobiol **2**, 127–153 (1983)
62. Harth, E., Tzanakou, E. ALOPEX: A stochastic method for determining visual receptive fields, Vision Research, Vol. 14, pp.1475–1482, (1974)
63. Haykin, S., Chen, Z., Becker, S. Stochastic correlative learning algorithms. IEEE Trans Signal Process, **52**(8) (Aug 2004)
64. Hindmarsh, J.L., Rose, R.M. A model of neuronal bursting using three coupled first order differential equations. Proc R Soc Lond B: Biol Sci **221**(1222), 87–102 March (1984)
65. Hodgkin, A.L., Huxley, A.F. A quantitative description of membrane current and its application to conduction and excitation in nerve. J Physiol **117**, 500–544 (1952)
66. Holmstrom, L., Koistinen, P., Laaksonen, J., Oja, E. Neural and statistical classifiers-taxonomy and two case studies. IEEE Trans Neural Netw **8**(1) Jan (1997)
67. Hopfield, J.J. Neural networks and physical systems with emergent collective computational abilities, Proc Natl Acad Sci USA **79,** 2554–2558 (1982)
68. House, W.F. Cochlear implants: My perspective, Dr. William F. House, 1995.
69. Humayun, M.S., de Juan E., Jr., Dagnelie, G., Greenberg, R.J., Propst, R.H., Phillips, D.H. Visual perception elicited by electrical stimulation of retina in blind humans. Arch Ophthalmol **114**(1) (1996)
70. Humphries, M.D., Gurney, K.N. A pulsed neural network model of bursting in the basal ganglia. Neural Netw **14**(6–7), 845–863 (2001)
71. Hurtado, J.M., Gray, C.M., Tamas, L.B., Sigvardt, K.A. Dynamics of tremor-related oscillations in the human globus pallidus: A single case study. Proc Natl Acad Sci USA **96**, 1674–1679 Feb (1999)
72. Iasemidis LD, Shiau DS, Pardalos PM, Chaovalitwongse, W., Narayanan, K., Prasad, A., Tsakalis, K., Carney, P.R., Sackellares, J.C. Long-term prospective online real-time seizure prediction. Clin Neurophys **116**(3), 532–544 (2005)
73. Izhikevich, E.M. Simple model of spiking neurons. IEEE Trans Neural Netw **14**, 1569–1572 Nov (2003)
74. Izhikevich, E.M. Which model to use for cortical spiking neurons? IEEE Trans Neural Netw **15**, 1063–1070 (2004)
75. Izhikevich, E.M. Which model to use for cortical spiking neurons. IEEE Transactions on Neural Netw **15**(5) (2004)
76. Jallabert, J. Experiences sur lectricit, Geneve, Barrillot & Fils (1748)
77. Joel, D., Niv, Y., Ruppin, E. Actor-critic models of the basal ganglia: New anatomical and computational perspectives. Neural Netw **15**, 535–547 (2002)
78. John, M.S. Adaptive brain stimulation method and system, US Patent#6463328, (2002)
79. Johnson, M.D., Otto, K.J., Kipke, D.R. Repeated voltage biasing improves unit recordings by reducing resistive tissue impedances. IEEE Trans Neural Syst Rehabil Eng **13**(2), 160–165 (2005)
80. Kaneko, H., Suzuki, S.S., Okada, J., Akamatsu, M. Multineuronal spike classification based on multisite electrode recording, whole-waveform analysis, and hierarchical clustering. IEEE Trans Biomed Eng **46**(3), March (1999)

81. Katz, B., Miledi, R. The measurement of synaptic delay, and the time course of acetylcholine release at the neuromuscular junction. Proc R Soc Lond, B Biol Sci **161**(985), 483–495 (Feb 16, 1965)
82. Kemere, C., Shenoy, K.V., Meng, T.H. Model-based neural decoding of reaching movements: A maximum likelihood approach. IEEE Trans Biomed Eng **51**(6) (Jun 2004)
83. Kilby, J.S. Miniaturized electronic circuits, US Patent #3138743, 1964.
84. Kimber, T.E., Tsai, C.S., Semmler, J., Brophy, B.P., Thompson, P.D. Voluntary movement after pallidotomy in severe Parkinson's disease, Brain **122**, 895–906 (1999)
85. Kite, C. An Essay on the Recovery of the Apparently Dead. C. Dilly, London (1788)
86. Kohler, B.U., Hennig, C., Orglmeister, R. The principles of QRS detection. IEEE Eng Med Biol Mag **21**(1), 42–57, Jan–Feb (2002)
87. Konstandinides, K., Tyree, V.C., Yao, K. Single chip implementation of the Levinson algorithm. IEEE J Solid-State Circuits **SC-20**(5) (Oct 1985)
88. Kulkarni, S.R., Lugosi, G., Venkatesh, S.S. Learning pattern classification—a survey. IEEE Trans Inform Theory **44**(6) (1998)
89. Kumar, R. Methods for programming and patient management with deep brain stimulation of the globus pallidus for the treatment of advanced Parkinson's disease and dystonia. Mov Dis **17**(3), S198–S207 (2002)
90. Lee, J., Rhew, H., Kipke, D., Flynn, M. A 64 channel programmable closed-loop deep brain stimulator with 8 channel neural amplifier and logarithmic ADC, 2008 Symposium on VLSI Circuits Digest of Technical Papers, pp.76–77 (2008)
91. Lehman, R.M., Micheli-Tzanakou, E., Medl, A., Hamilton, J.L. Quantitative online analysis of physiological data for lesion placement in pallidotomy. Stereotact Funct Neurosurg **75**(1), 1–15 (2000)
92. Lenz, F.A., Kwan, H.C., Martin, R.L., Tasker, R.R., Dostrovsky, J.O., Lenz, Y.E. Single unit analysis of the human ventral thalamic nuclear group. Tremor related activity in functionally identified cells. Brain **117**(3), 531–543 (1994)
93. Liao, H., Mandal, M.K., Cockburn, B.F. Efficient architectures for 1D and 2D lifting-based wavelet transforms. IEEE Trans Signal Process **52**(5) (May 2004)
94. Licht, S. Therapeutic Electricity and Ultraviolet Radiation. New Haven, E. Licht (1967)
95. Malmivuo, J., Plonsey, R. Bioelectromagnetism, Principles and Applications of Bioelectric and Biomagnetic Fields. Oxford University Press, New York (1995)
96. Manolakos, E.S., Stellakis, H.M. Systematic synthesis of parallel architectures for the computation of higher order cumulants. Parall Comput **26**, 655–676 (2000)
97. Matteuci, C. Sur un phenomene physiologique produit par les muscles en contracion, Annales de Chimie et de Physique, 6(339) (1842)
98. McCulloch, W.S., Pitts, W.H. A logical calculus of the ideas immanent in nervous activity. Bull Math Biophys **5**, 115–133 (1943)
99. McIntyre, C.C., Grill, W.M. Extracellular stimulation of central neurons: Influence of stimulus waveform and frequency on neuronal output. J Neurophysiol **88**, 1592–1604 (2002)
100. McIntyre, C.C., Grill, W.M. Excitation of central nervous system neurons by nonuniform electric fields. Biophys J **76**, 878–888 (Feb 1999)
101. McIntyre, C.C., Thakor, N.V. Uncovering the mechanisms of deep brain stimulation for Parkinson's disease through functional imaging, neural recording and neural modeling. Crit Rev Biomed Eng **30**(4–6), 249–281 (2002)
102. Medtronic Corporation, Extension kit for deep brain stimulation, spinal cord stimulation, or peripheral nerve stimulation, implant manual, Medtronic, Inc. (2002)
103. Meissimilly, G., Rodriguez, J., Rodriguez, G., Gonzalez, R., Canizares, M. Microcontroller-based real-time QRS detector for ambulatory monitoring. Proc IEEE Eng Med Biol Soc **3**, 17–21 (2003)
104. Micheli-Tzanakou, E., Hamilton, J., Zheng, J., Lehman, R. Computational intelligence for target assessment in Parkinson's disease. In: Bosacchi, B., Fogel, D.B., Bezdek, J.C. (eds.) Proceedings of the SPIE, Applications and Science of Neural Networks, Fuzzy Systems, and Evolutionary Computation IV, Vol. 4479, pp. 54–69. SPIE-Medical Imaging (2001)

105. Micheli-Tzanakou, E., Michalak, R., Harth, E. The Alopex process: Visual receptive fields with response feedback. Biol Cybern **35**, 161–174 (1979)
106. Montgomery, E.B., Jr., Baker, K.B. Mechanisms of deep brain stimulation and future technical developments. Neurol Res **22**, 259–266 (2000)
107. Moore, G.E. Cramming more components onto integrated circuits. Electronics **38**(8) (1965)
108. Moxon, K.A., Kalkhoran, N.M., Markert, M., Sambito, M.A., McKenzie, J.L., Webster, J.T. Nanostructured surface modification of ceramic-based microelectrodes to enhance biocompatibility for a direct brain-machine interface. IEEE Trans Biomed Eng **51**(6) (June 2004)
109. Mraz, S.J. Rewiring the retina. Machine Design **75**(13), 60–64 (Jul 10, 2003)
110. Muenter, M.D., Tyce, G.M. l-dopa therapy of Parkinson's disease: Plasma l-dopa concentration, therapeutic response, and side effects. Mayo Clin Proc **46**, 231–239 (1971)
111. Nicolelis, M.A.L. Brain machine interfaces to restore motor function and probe neural circuits. Nat Rev Neurosci **4**(5), 417–422 (2003)
112. Noble, D. A modification of the Hodgkin-Huxley equations applicable to purkinje fibre action and pacemaker potentials. J Physiol **160**, 317–352 (1962)
113. Novo, A., Gerosa, A., Neviani, A. A sub-micron CMOS programmable charge pump for implantable pacemaker. Analog Integrated Circuits Signal Process **27**, 211–217 (2001)
114. Noyce, R.N. Semiconductor device-and-lead structure, US Patent # 2981877, 1961.
115. Nutt, J., Anderson, V.C., Peacock, J.H., Hammerstad, J.P., Burchiel, K.J. DBS and diathermy interaction induces severe CNS damage. Neurology **56**, 1384–1386 (2001)
116. Pardo, M., Sberveglieri, G. Learning from data: A tutorial with emphasis on modern pattern recognition methods. IEEE Sens J **2**(3), 203–217 (2002)
117. Patterson, W.R., Song, Y., Bull, C.W., Ozden, I., Deangellis, A.P., Lay, C., McKay, J.L., Nurmikko, A.V., Donoghue, J.D., Connors, B.W. A microelectrode/ microelectronic hybrid device for brain implantable neuroprosthesis applications. IEEE Trans Biomed Eng **51**(10) (Oct 2004)
118. Peng, H., Long, F., Ding, C. Feature selection based on mutual information: Criteria of max-dependency, max-relevance, and min-redundancy. IEEE Trans Pattern Anal Mach Intell **27**(8), 1226 (2005)
119. Pea, C., Bowsher, K., Costello, A., De Luca, R., Doll, S., Li, K., Schroeder, M., Stevens, T. An overview of FDA medical device regulation as it relates to deep brain stimulation devices. IEEE Trans Neural Syst Rehabil Eng **15**(3), 421–424 (2007)
120. Plenz, D., Kitai, S. A basal ganglia pacemaker formed by the subthalamic nucleus and external globus pallidus. Nature **400**, 677–682 (1999)
121. Priestley, J. The history and present state of electricity: With original experiments. Printed for C. Bathurst, and T. Lowndes . . . J. Rivington, and J. Johnson . . . S. Crowder, G. Robinson, and R. Baldwin . . . T. Becket, and T. Cadell . . ., London, MDCCLXXV (1775)
122. Pudil, P., Novovicova, J., Somol, P. Feature selection toolbox software package. Pattern Recognit Lett **23**, 487–492 (2002)
123. Eckmiller, R., Eckhorn, R. Final report of the feasibility study for a neurotechnology program, NeuroTechnology Report, BMBF, Bonn, Germany (1994)
124. Rajasekaran, S. Efficient parallel algorithms for template matching. Parallel Process Lett **12**(3–4), 359–364 (2002)
125. Rall, W., Burke, R.E., Holmes, W.R., Jack, J.J., Redman, S.J., Segev, I. Matching dendritic neuron models to experimental data. Physiol Rev **72**(4) (Suppl), S159–S86 (1992)
126. Raz, A., Vaadia, E., Bergman, H. Firing patterns and correlations of spontaneous discharge of pallidal neurons in the normal and the tremulous 1-methyl-4-phenyl-1,2,3,6-tetrahydropyridine vervet model of parkinsonism. J Neurosci **20**(22), 8559–8571 (Nov 15, 2000)
127. Rise, M.T., King, G.W. Method of treating movement disorders by brain stimulation, US Patent #5716377 (1998)
128. Rodrigues, J.N., Owall, V., Sornmo, L. A wavelet based R-wave detector for cardiac pacemakers in 0.35 CMOS technology, IEEE Circuits Syst Proc (ISCAS) **4**, 23–26 (2004)
129. Rosenblatt, F. The perceptron: A probabilistic model for information storage and organization in the brain. Psychol Rev **65**(6), 386–408 (1958)

130. Rossi, L., Marceglia, S., Foffani, G., Cogiamanian, F., Tamma, F., Rampini, P., Barbieri, S., Bracchi, F., Priori, A. Subthalamic local field potential oscillations during ongoing deep brain stimulation in Parkinson's disease. Brain Res Bull **76**(5), 512–521 (2008)
131. Ruggera, P.S., Witters, D.M., Maltzahn, G., Bassen, H.I. In vitro assessment of tissue heating near metallic medical implants by exposure to pulsed radio frequency diathermy. Phys Med Biol **48**, 2919–2928 (2003)
132. Sanchez, J.C., Sung-Phil, K., Erdogmus, D., Rao, Y.N., Principe, J.C., Wessberg, J., Nicolelis, M. Input-output mapping performance of linear and nonlinear models for estimating hand trajectories from cortical neuronal firing patterns. Proceedings of the 12th IEEE Workshop on Neural Networks for Signal Processing, 4–6, 139–148 (Sep. 2002)
133. Sanders, R.S., Lee, M.T. Implantable pacemakers. Proc IEEE **84**(3), 480–486 (March 1996)
134. Sanghavi, T. Design of an alopex architecture and its application to adaptive deep brain stimulation (ADBS), Rutgers theses. Graduate Program in Electrical and Computer Engineering (2005)
135. Sastry, P.S., Magesh, M., Unnikrishnan, K.P. Two timescale analysis of the ALOPEX algorithm for optimization. Neural Comput, 14, 2729–2750 (2002)
136. Scharstein, H. Input–output relationship of the leaky-integrator neuronmodel. J Math Biol **8**(4), 403–420 (1979)
137. Schueler, B.A., Parrish, T.B., Lin, J., Hammer, B.E., Pangrle, B.J., Ritenour, E.R., Kucharczyk, J., Truwit, C.L. MRI compatibility and visibility assessment of implantable medical devices. J Mag Res Imaging **9**, 596–603 (1999)
138. Schweigger, J.S.C. Zustze zu ersteds elektromagnetischen versuchen, vorgelesen in der naturforschenden. Journal fr Chemie und Physik, Schweigger Ed. **31**(1–17), 431 (1821)
139. Scribonius, L. Compositiones. In: Sergio Sconocchia (ed.) Scribonii Largi Compositiones. Teubner, Leipzig (1983)
140. Sejnowski, T.J. The book of Hebb. Neuron **24**, 773–776 (1999)
141. Shinomoto, S., Kuramoto, Y. Phase transitions in active rotator systems. Prog Theor Phys **75**, 1105–1110 (1986)
142. Sridhar, A. Analog CMOS Model of Parkinson's Disease, Thesis (M.S.), Rutgers University (2005)
143. Stein, R.B. A theoretical analysis of neuronal variability. Biophys J **5**, 173–194 (1965)
144. Struijk, J.J. Thomsen, M., Larsen, J.O. Sinkjaer, T. Cuff electrodes for longterm recording of natural sensory information. IEEE Eng Med Biol Mag **18**(3), pp. 91–98 (1999)
145. Suri, R.E. Albani, C., Glattfelder, A.H. A dynamic model of motor basal ganglia functions. Biol Cybern **76**(6), 451–458 (1997)
146. Tass, P.A. Amodel of desynchronizing deep brain stimulation with a demand controlled coordinated reset of neural subpopulations. Biol Cybern **89**(2), 81–88 (August 2003)
147. Tass, P.A. Effective desynchronization with bipolar double-pulse stimulation. Phys Rev E **66**, 036226 (2002)
148. Taylor JG, Taylor NR. Analysis of recurrent cortico-basal ganglia-thalamic loops for working memory. Biol Cybern **82**(5), 415–432 (2000)
149. Terman, D., Rubin, J.E., Yew, A.C., Wilson, C.J. Activity patterns in a model for the Subthalamopallidal Network of the Basal Ganglia. J Neurosci **22**, 2963–2976 (2002)
150. Tzanakou, E., Harth, E. Determination of visual receptive fields by stochastic methods. Biophys J **15**, 42a (1973)
151. U.S. Department of Health and Human Services. FDA approves implanted brain stimulator to control tremor, Press Release P97–24 (August 4, 1997)
152. Volkmann, J., Herzog, J., Kopper, F., Deuschl, G. Introduction to the programming of deep brain stimulators. Mov Dis **17**(Suppl. 3), S181–S187 (2002)
153. Volta, A. On the electricity excited by the mere contact of conducting substances of different kinds. Philosophical Trans **90**, part 2, 403–431, with one folding engraved plate, numbered XVII, (1800)
154. Warman, E.N., Grill, W.M., Durand, D. Modeling the effects of electric fields on nerve fibers: Determination of excitation thresholds. IEEE Trans Biomed Eng, **39**(12) (Dec. 1992)

155. Wessberg, J., Stambaugh, C.R., Kralik, J.D., Beck, P.D., Laubach, M., Chapin, J.K., Kim, J., Biggs, S.J., Srinivasan, M.A., Nicolelis, M.A.L. Real-time prediction of hand trajectory by ensembles of cortical neurons in primates. Nature **408**, 361–365 (November 16, 2000)
156. Wichman, T., DeLong, M.R. Pathophysiology of Parkinsons disease: The MPTP primate model of the human disorder. Ann NY Acad Sci **991**, 199–213 (2003)
157. Wilson, H.R. Simplified dynamics of human and mammalian neocortical neurons. J Theor Biol **200**, 375–388 (1999)
158. Wingeier, B., Tcheng, T., Koop, M.M., Hill, B.C., Heit, G., Bronte-Stewart, H.M. Intra-operative STN DBS attenuates the prominent beta rhythm in the STN in Parkinson's disease. Exp Neurol **197**, 244–251 (2006)
159. Wise, K.D., Anderson, D.J., Hetke, J.F., Kipke, D.R., Najafi, N. Wireless implantable microsystems: High-density electronic interfaces to the nervous system. Proc IEEE **92**(1) (January 2004)
160. Wolpert, S., Micheli-Tzanakou, E. A neuromime in VLSI. IEEE Trans Neural Netw **7**(2) (March 1996)
161. Wu, W., Black, M.J., Gao, Y., Bienenstock, E., Serruya, M., Shaikhouni, A., Donoghue, J.P. Neural decoding of cursor motion using Kalman filtering. In: Becker, S., Thrun, S., Obermayer, K. (eds.) Advances in Neural Information Processing Systems, Vol. 15, pp.117–124. MIT Press, Cambridge (2003)
162. Wu, Y.R., Levy, R., Ashby, P., Tasker, R.R., Dostrovsky, J.O. Does stimulation of the GPI control dyskinesia by activating inhibitory axons? Mov Dis **16**(2), 208–216 (2001)